SUPPRESSING HARMONICS IN STANDING-WAVE THERMOACOUSTIC ENGINES

A.H. Ibrahim[1], A.A. Elbeltagy, M. Emam[1], Moamen Abdou, Hosny Omar and Ehab Abdel-Rahman[+]

Physics Department, School of Sciences and Engineering, American University in Cairo
11835 New Cairo, Egypt
[+] Corresponding author: ehab_ab@aucegypt.edu

Thermoacoustic engines convert heat to acoustic power using the rich interactions between thermodynamics and acoustics. These engines operate with inert gases with no moving parts and thus enjoy high reliability and low cost. Operating these engines at high temperatures is essential for high conversion efficiency but non-linearities have to be controlled. One of the main sources of non-linearity is the generation of harmonics, which extract acoustic power from the fundamental wave. This work studies the use of specifically-designed inserts to suppress the generation of harmonics. Inserts of different shapes, porosities, thicknesses are positioned along the standing-wave in an otherwise iso-diameter resonator. The results indicate that largest suppression occurs when the insert is positioned at the velocity anti-node of the first harmonic. Among different shapes considered, the insert of porosity of 50% open area distributed over several circles is found to suppress harmonics more than other studied porosities or shapes. Results on the harmonic content, acoustic power in the fundamental and first harmonics, pressure and temperature distributions are presented for cases without inserts and with different insert shapes. Results comparing the engine performance with and without inserts for the identified best insert configuration are presented when the engine is operated with a gas mixture made of 80% and 20% argon at mean atmospheric pressure.

1 Introduction

Thermoacoustics is a promising technology that has a rapidly growing field of applications. Thermal engines and refrigerators based on the manipulation of temperature variations on the acoustic standing wave can be safe and durable. In any sound wave, there exist coupled pressure and displacement oscillations. The pressure oscillations induce temperature oscillations which in turn cause heat flow to or from nearby surfaces.

A standing-wave thermoacoustic engine is a thermoacoustic device that converts heat into mechanical work in the form of standing-wave acoustic oscillations. The thermodynamic cycle inside the engine follows the pressure volume variations similar to a Brayton cycle. If a high enough heat gradient is imposed on the stack of the thermoacoustic engine, the working gas starts to exhibit self-induced oscillations once a certain temperature gradient, known as the critical temperature gradient, across the stack is reached. This generates a standing acoustic wave in the resonator where the stack is contained. The necessary temperature gradient is imposed by two heat exchangers surrounding the stack. A hot-side heat exchanger supplies heat to one side of the stack, possibly from solar energy or waste heat, and a

[1] On leave from Mechanical Power Department, Faculty of Engineering, Cairo University, Giza, Egypt

cold-side heat exchanger has to remove heat from the other-side of the stack to maintain the temperature gradient across the stack and sustain the energy conversion.

Prototypes of these engines have demonstrated first and second law efficiencies of 18% and 30%, respectively [1], [2]. Operations with solar energy as well as waste heat were demonstrated [3], [4]

Thermoacoustic engines have notable advantages: The gas oscillations in the engine are produced without a piston arrangement inside the resonator. This eliminates the need to use mechanical seals or lubricants and ensures high reliability and low cost; the working fluid in this type of energy converter is typically an inert gas or gas mixture, which is inherently safe and environmentally-friendly and does not cause global warming effects; the engine easily can be driven with solar or waste heat sources and different designs of the engine or different gas mixtures on the same engine design can be used to accommodate different heat sources [5]. Moreover, small sizes of TAE can be built to provide a portable source of electricity, and several TAE's can be coupled together to increase the total acoustic power [6].

However, these engines require efficient heat exchangers to ensure proper heat supply and heat removal to and from the stack. An inadequate heat exchanger on the hot stack side limits the heat rate supplied to the stack and consequently the resulting acoustic power produced. On the other side, an inadequate heat exchanger on the cold side fails to sustain the temperature gradient across the stack, which is critical for sustainable operation. In addition, these engines usually utilize gas mixtures of significant light gas component at relatively high mean pressures (up to 40 bar), which creates a sealing issue. But the main challenges remain the relatively low conversion efficiency and the relatively low power density. To increase the conversion efficiency, operation at high temperatures is essential, as dictated by the second law of thermodynamics [7].

Operation at temperatures much higher than the onset temperature causes significant part of the generated acoustic power to be carried out in the harmonics rather than the fundamental mode. Because the load on the engine, like a linear alternator or a thermoacoustic refrigerator, only can benefit from power carried out in the fundamental mode, harmonic generation is regarded as a major loss mechanism and should be eliminated or reduced. Operation at temperatures slightly higher than the onset temperature has been shown to reduce harmonic generation [5], but use of high temperatures is essential, from a second-law perspective, for high conversion efficiency. Thus generation of harmonics must be eliminated or reduced.

The generated pressure wave has non-linearities due to the non-linear nature of the fluid flow behaviour. The harmonics are generated because of the non-linear terms in the Navier-Stokes equations, such as the product of the dynamic density and the gas parcel velocity, which are both first-order terms. Each of these terms has a $cos(\omega t)$ dependence, and their product causes a $cos(2\omega t)$ dependence because $cos(\omega t) \times \cos(\omega t) = 0.5[1 + cos(2\omega t)]$. Once the $(2\omega t)$ waves are generated, they interact with the fundamental mode oscillating at the angular frequency ω, giving rise to a weaker 3ω oscillations because $cos(\omega t) \times \cos(2\omega t) = 0.5[cos(\omega t) + cos(3\omega t)]$.

The harmonics are multiple integers of each other. For an iso-diameter resonator, where the cross-sectional area is independent of the axial location along the entire length, the resonance frequencies of the resonator are multiple integers of the fundamental. The harmonics also are generated as multiple integers from the fundamental as well causing the harmonics to *coincide* with resonance frequencies and to get amplified.

The insert makes the resonance frequencies of the engine not as multiple integers of each others. The harmonics are still generated at multiple integers of the fundamental frequency but now the harmonics do not coincide with a resonance frequency and thus they do not get amplified and are significantly reduced. This work focuses on *one* method to reduce harmonic generation, which is the use of specifically-designed inserts positioned at the velocity anti-node of the first harmonic. In this work, different inserts are investigated with different porosities and different shapes. Other methods involve the use of tapered or anharmonic resonators [8], [9]. Variable-diameter resonators where the stack is positioned at the large diameter part provide another advantage by reducing the viscous losses.

This work utilizes a simple method to reduce the harmonics. The method is to place specifically-designed inserts of lower flow area inside the resonator at the velocity anti-node of the first harmonic to suppress its formation. This suppression is evaluated by observing the shape of the generated sine wave in the time domain, the intensity of the spectral density of its fast Fourier transform (FFT) in the

frequency domain. The generated wave is then decomposed into a fundamental and a set of harmonics using curve fitting. Knowing the magnitudes and phases of the dynamic pressures in the fundamental and the different components allows estimation of the acoustic power carried out in the fundamental mode and in the first harmonics. Then, the acoustic powers carried out in the fundamental and in the first harmonic, the intensity of the dynamic pressure of the fundamental, first and second harmonics are compared for the cases with and without inserts and are used as indicators of the harmonic suppression.

2 Experimental setup

A schematic of the experimental setup is shown in figure 1. The wavelength in this experiment is 1.86 m. The engine consists of a resonator (made of steel except the hot part made of stainless steel, 0.5λ length, 0.068λ inside diameter, closed at both sides) housing a stack surrounded by two heat exchangers. The stack is the main thermoacoustic element through which the energy conversion occurs. The stack is 3 cm long, has 400 cells per square inch, has a wall thickness of $0.065\delta_k$ and a wall spacing of $0.48\delta_k$ where δ_k is the thermal penetration depth, is made of celcor and is supplied by Corning. The stack is positioned between two home-made heat exchangers. One side of the stack is heated using an electric heater connected to a voltage divider (2 kVA Power rating) to allow control of the input electric power fed to the engine and corresponding control of the hot-side temperature of the stack. The heater can be considered as a resistive component with a resistance of 28.8 Ω. To maintain the temperature gradient across the stack, the other side of the stack is cooled via a home-made heat exchanger made of eleven-path 6-mm inside diameter copper tubes with copper fins. The water flow rate through this heat exchanger at the operating conditions used in this work is 270 ml/s and the cold heat exchanger is found to be able to sustain the temperature gradient across the stack. During the current study, the stack is kept at 0.037λ away from the hot-side blind flange.

To fill the engine with gases other than air, the atmospheric air is first pumped out using a vacuum pump, and then the required gas or gas mixture is filled using helium or argon cylinders (purity 99.99 % and 99.0 %, respectively). The gases then are purged using the vacuum pump and fresh helium/argon gas is refilled again. The purging process is repeated three times to fully remove the air traces inside the engine and then the required gas mixture is filled in the engine. Two working fluids are used in this work. The first is a mixture of 80% argon 20% helium and the second is air. Both working fluids are used at a mean pressure of one atmospheric pressure.

The temperatures at the hot and cold sides of the stack are measured with type K thermocouples. The pressure microphones used are piezo-resistive Meggitt microphones (Model 8510B-2, range 0-2 psi gage, individually calibrated, sensitivity of about 20 mV/kPa and a resonance frequency of 70 kHz). The signals from the pressure transducers are fed into a three-channel, 200-kHz bandwidth, programmable-gain DC amplifier. Both temperature and pressure signals are acquired simultaneously using a USB data acquisition board (DAQ NI USB-6343, 16-bit, 16 differential channels, 1-MHz band width, with programmable gain).These measurements allow capturing of the hot and cold stack temperatures as well as the resultant dynamic pressure amplitude at different axial locations. This data allows decomposition of the produced wave into fundamental and harmonics and estimation of the acoustic power carried out in the fundamental mode and in the first harmonics using the two-microphone method [10].

The inserts used in this apparatus were made of two different open (gas) areas: 0.75 and 0.5 of the resonator area. The insert thickness is 0.016λ, which is small enough compared to the wave length (1.86 m). The insert open area was in form of an open ring or a ring of multiple holes. The different inserts used are shown in figure 2.

Every experiment is named as XYT-Z, where X is the gas area as a percentage of the resonator area, Y is the shape code: either A which is a hollow ring or C which is multiple holes, T is the insert thickness and Z is the insert position from the hot-side blind flange. For example, the insert labeled as 50C3-68 consists of multiple holes, with an open area of half the area of the resonator area, a thickness of 3 cm (0.016λ), and the insert is placed at 68 cm (0.37λ) away from the hot-side blind flange.

The excitation of harmonics is evaluated through the wave decomposition into a fundamental mode and higher harmonics, through nonlinear curve fitting in Matlab by reducing the sum of squared-

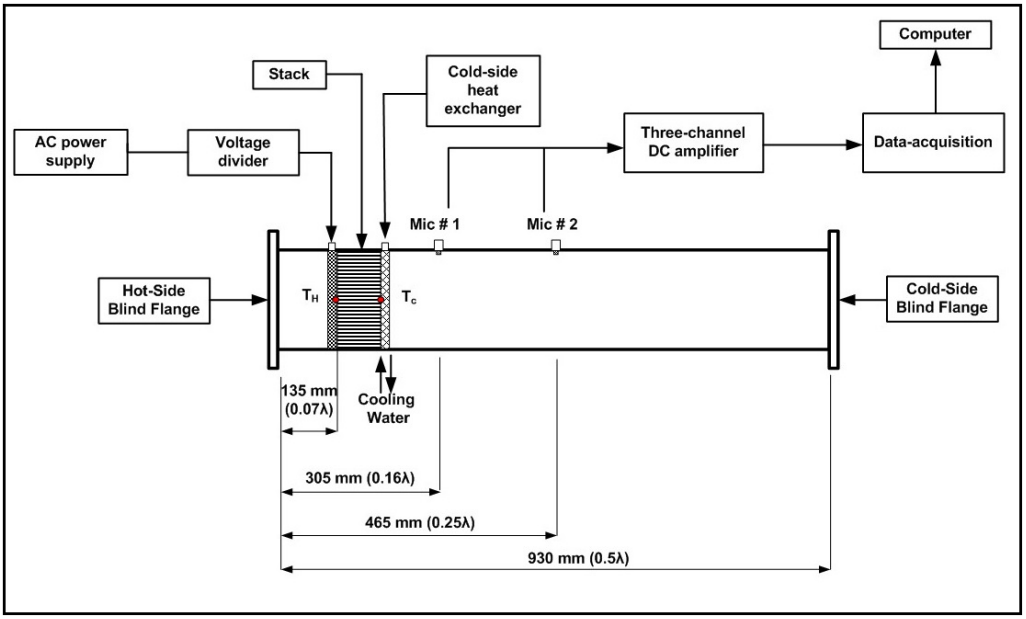

Figure 1: A schematic of the thermoacoustic engine and its measuring instruments (Not to scale).

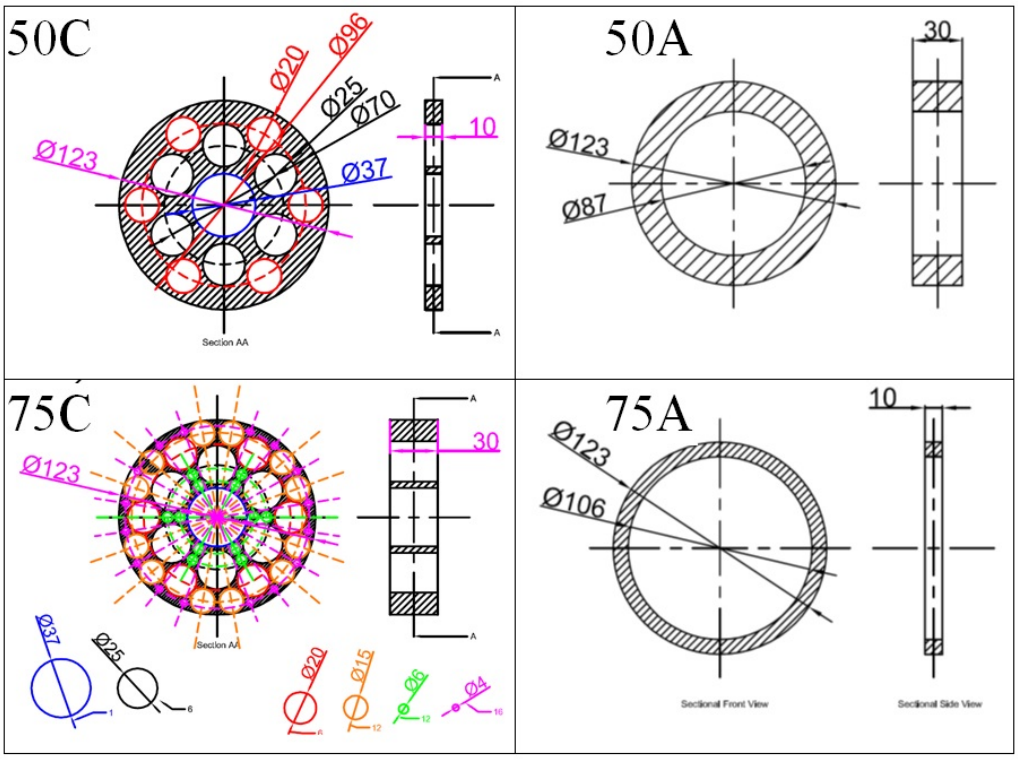

Figure 2: The shapes and labels of the inserts used in this experiment.

deviations between the measured signal and the above numerical form as shown in Equation 1

$$P(t) = P_0 sin(2\pi f_0 t + \phi_0) + P_1 sin(2\pi f_1 t + \phi_1) + P_2 sin(2\pi f_2 t + \phi_2) + P_3 sin(2\pi f_3 t + \phi_3) \quad (1)$$

3 Results and discussion

This section presents raw and analyzed data for engine operation with and without different types of inserts.

3.1 Effects of insert usage

To investigate the effects of the introduction of the insert in the resonator, the engine is operated with and without the insert and the results are presented and compared. This section presents the results obtained when the engine is operated using a mixture of 80% Argon and 20% Helium at atmospheric mean pressure, operating with heat rate in the range of 125 W to 1681 W.

Figure 3 shows the measured pressure points as symbols and the curve-fitted wave as curve, confirming the high accuracy of the curve fitting process. The figure shows the standing pressure wave produced by the engine when operated using a mixture of 80% Ar and 20% He without (top figure) and with (bottom figure) insert 50C3-68. The figure shows the generated pressure signal in the time domain when the engine is operated at its maximum heat input rate (1681 W). Non linearities appear the most at the highest input heat rate and clear harmonic distortion can be observed in the time domain representation of the signal. The figure shows that when the insert 50C3-68 (porosity of 50% divided into multiple holes, thickness of 3 cm, and positioned at 68 cm away from the hot-side blind flange) is used, the harmonic distortion in the time domain is clearly reduced (Figure 3a versus 3b).

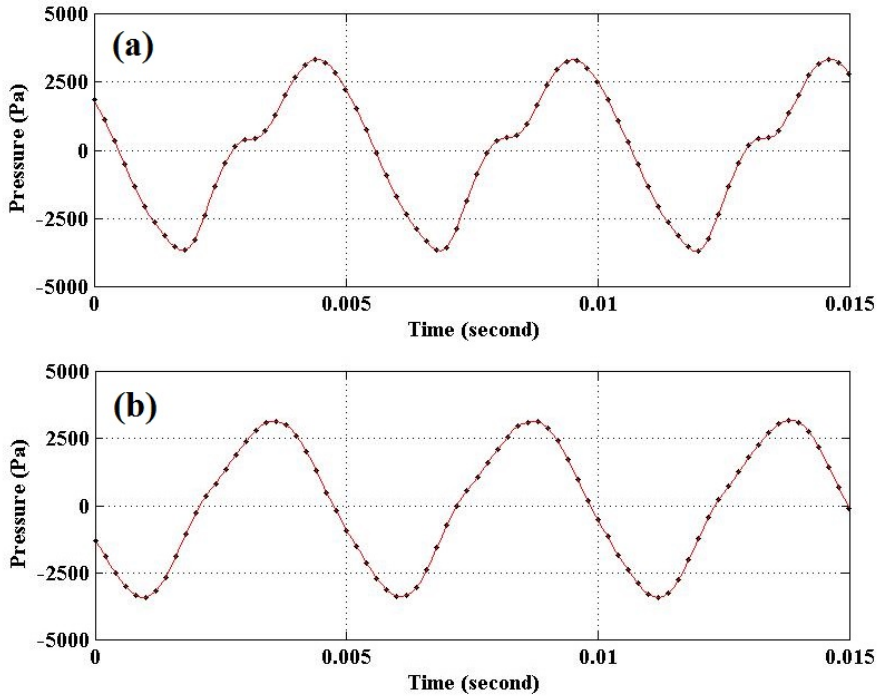

Figure 3: The standing pressure wave produced by the engine when operated without the insert (top figure) and with the insert 50C3-68 (bottom). Engine operated at its maximum heat input rate (1681 W)

Figure 4 shows the FFT of the same signal indicating the existence of the fundamental frequency (195.3 Hz), followed by the first, second, and third harmonics (at 390.6 Hz, 590.8 Hz, and 786.1 Hz, respectively). The spectral density of the first harmonic is about 2.3% of that of the fundamental. The spectral density of the second harmonic is about 55% of the first. This ratio is 15% between the third and second harmonics and is about 5% between the fourth and the third harmonics. This shows how acoustic energy is divided into the fundamental mode and different harmonics.

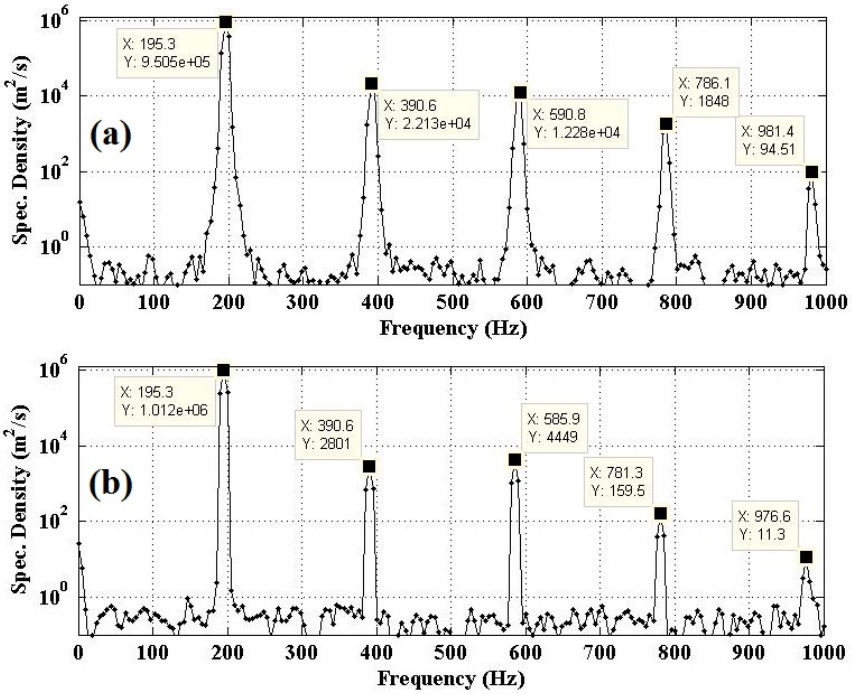

Figure 4: Fast Fourier transform for the pressure waves shown in figure 3, without (top) and with 50C3-68 insert (bottom)

The effect of the insert is further seen by observing the spectral density of the pressure signal in the fundamental mode and in the harmonics (Figure 4a versus 4b): With the insert used, the spectral density of the first harmonic is 0.28% of that of the fundamental mode, as opposed to 2.3% in the no-insert case. This is about eight times improvement in this value. The spectral density of the second harmonic is 159% of that of the first, as opposed to 55% in the no-insert case. This is due to extreme reduction in the amplitude of the first harmonic in particular because the insert is placed right at the velocity anti-node of the first harmonic specifically. The spectral density of the third harmonic is 3.6% of that of the second, as opposed to 15% in the no-insert case. The spectral density of the fourth harmonic is 7.1% of that of the third, as opposed to 5% in the no-insert case. In all cases, clear reduction in the absolute values of the dynamic pressures of all harmonics have reduced significantly as compared with the no-insert case, as shown in figure 5.

Figure 6 shows the measured acoustic power in the fundamental mode versus the input heat and the corresponding DeltaEC simulation. It is noticed that the DeltaEC simulation for the acoustic power are much higher than the measured values due to the many losses that occur experimentally and are not accounted for numerically such as heat losses from the heater, inefficient heat exchangers, harmonic generation and streaming. The same figure also shows that the use of the insert causes a clear increase in the acoustic power carried in the fundamental, together with a clear reduction in the power carried in the first harmonic, as depicted in Figure 6. For example, at the largest input heat rate (1681W), the acoustic power carried out in the fundamental mode increased from 3.44 W to 8.36 W after the placement of the insert while that carried out in the first harmonic decreased from 1.28 W to 0.12 W after the placement of the insert.

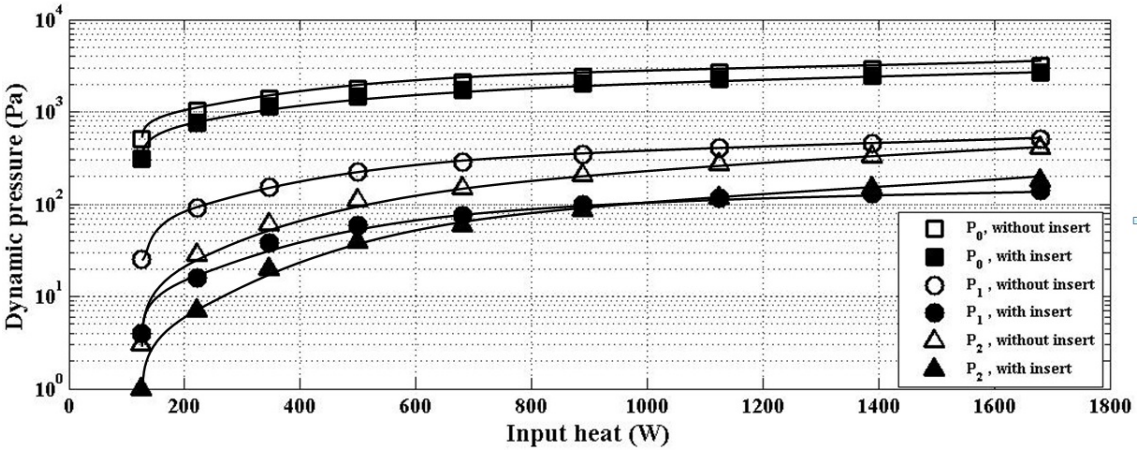

Figure 5: Development of dynamic pressures of the fundamental mode, first and second harmonics with the input heat rate, with and without 50C3-68 insert

The linear theory [11] predicts that the square of the fundamental dynamic pressure (P_0^2) is proportional to the input heat rate, which is observed in Figure 7. This suggests that the excess heat transported by the first harmonic is proportional to the square of the dynamic pressure of the first harmonic. This means that a two-fold reduction in the dynamic pressure of the first harmonic yields a four-fold reduction in the excess heat transported by the first harmonic [12]

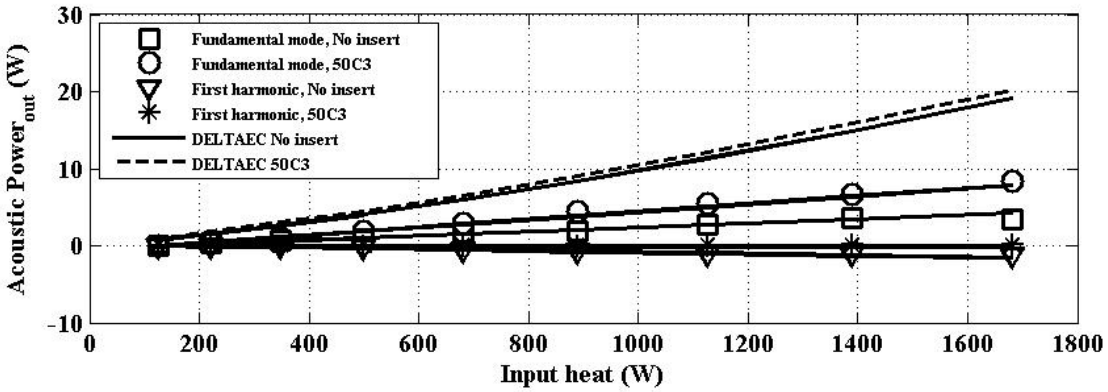

Figure 6: Acoustic power generated in fundamental and first harmonic and DeltaEC comparisons, with and without insert

Although the placement of the insert increases the acoustic power in the fundamental mode, it affects the dynamic pressure and the mean gas temperatures. These effects are quantified in figure8. The figure shows that the dynamic pressure of the fundamental mode is slightly reduced due to blockage while the dynamic pressure of the first harmonic is severely reduced. The insert causes some slight changes to the mean gas temperature as shown in the figure. The use of inserts 25A3 or 25C3 causes a severe increase in the mean gas temperature to the limit that may impact the engine mechanical parts.

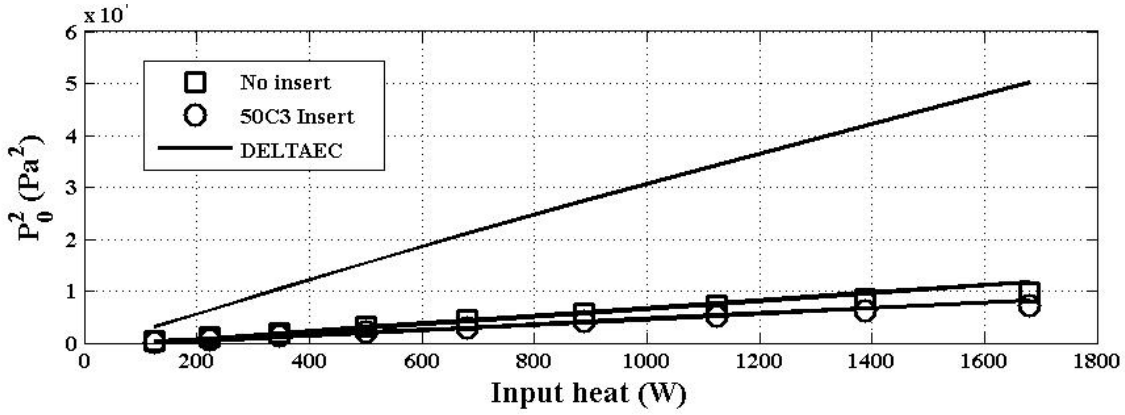

Figure 7: Linear relationship between the square of the fundamental of the dynamic pressure versus the input heat rate, with and without 50C3-68 insert, and DeltaEC comparison.

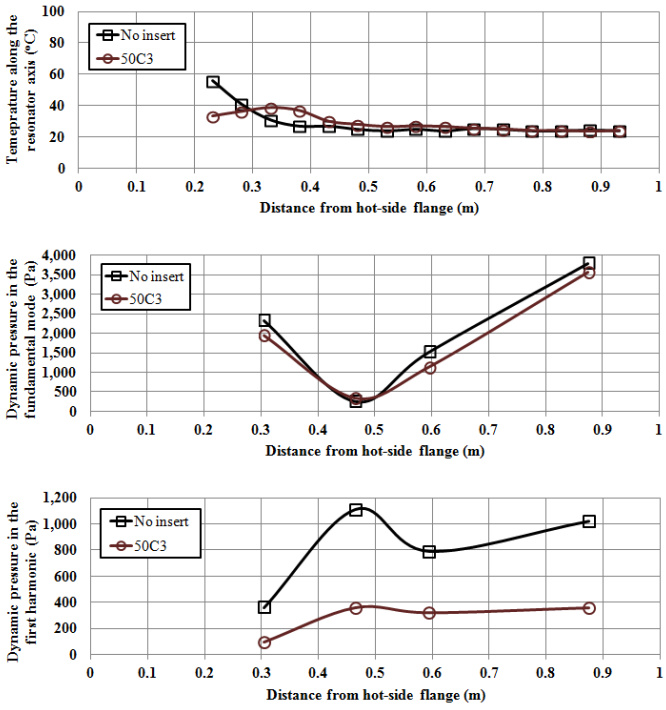

Figure 8: Distribution of dynamic pressure and mean gas temperature along the engine axis without and with 50C3-68 insert. The working fluid is 80% argon 20% helium

Further harmonic analysis is shown in Figures 9a and 9b expressing linear relationship between the dynamic pressure of the first harmonic P_1 and P_0^2 and another linear relationship between the dynamic pressure of the second harmonic P_2 and P_1^2. This figure shows an example on how the linear relationship holds until the input heat rate is high enough causing the measurements to fall below the linear fit. More data and analysis on this issue can be found in [13], [14]

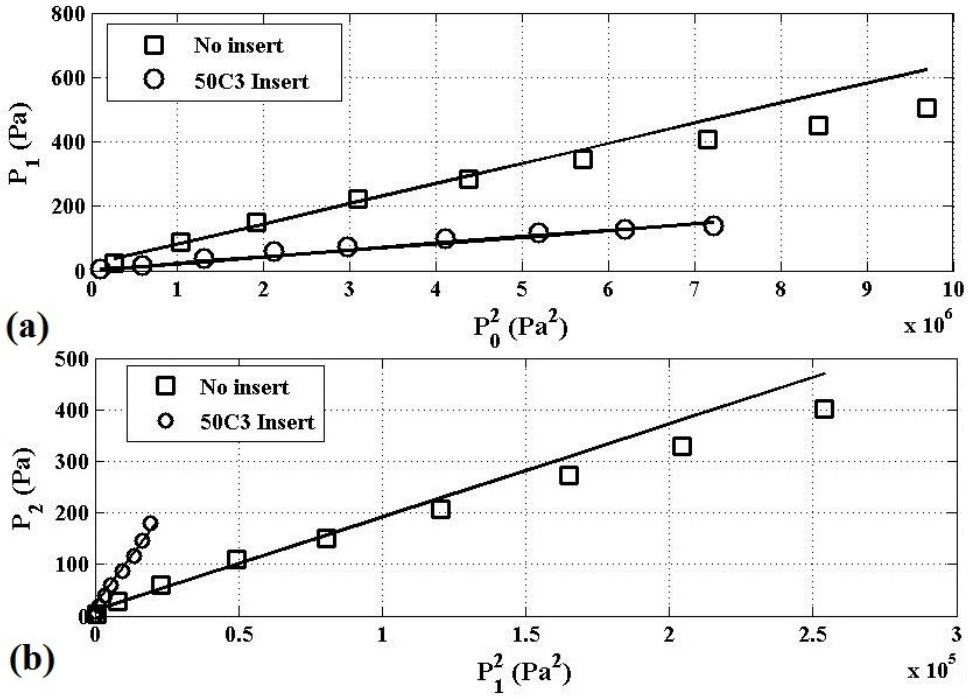

Figure 9: Linear relationships in harmonic amplitudes with and without insert; (a) P_1 with P_0^2 and (b) P_2 with P_1^2, with and without 50C3-68 insert

The reduction in P_1 versus P_o^2 is shown in Figure 9a where at the highest input heat rate, the value of P_1 decreased from 504 Pa to 139.46 Pa after the placement of the insert.

Figure 9b shows that for the same P_1^2, P_2 increases due to the placement of the insert, although the absolute value of P_2 itself decreases. This is consistent with the observation made in the frequency domain before. Careful observation of the absolute pressure values, shown in figure 5 shows that all the components of the dynamic pressure are reduced with the use of the insert, particularly the first harmonic where the insert is positioned at its velocity anti-node.

3.2 Effects of insert shape, porosity, and position

The current work studies inserts of two different porosities, 75% open area and 50% open area. Two different shapes are considered within each porosity, either a *C* shape where the open area is divided into several circles or an *A* shape where the open area is collected in one hollow circle, as shown in Figure 2.

Figures 10, 11, and 12 present the acoustic power carried out in the fundamental mode and in the first harmonic as well as the frequency of operation for each of the four inserts considered. During the preliminary tests, an insert with a small porosity (25%) was tried but it caused a severe increase in the hot and cold stack side temperatures and a low acoustic power output so it was eliminated.

The figures show that the placement of the different inserts in the resonator results in an increase in acoustic power in fundamental wave, and a decrease in acoustic power in the first harmonic. The frequency, shown in figure 12, was minimum for the case with the maximum power. However, the 50C3

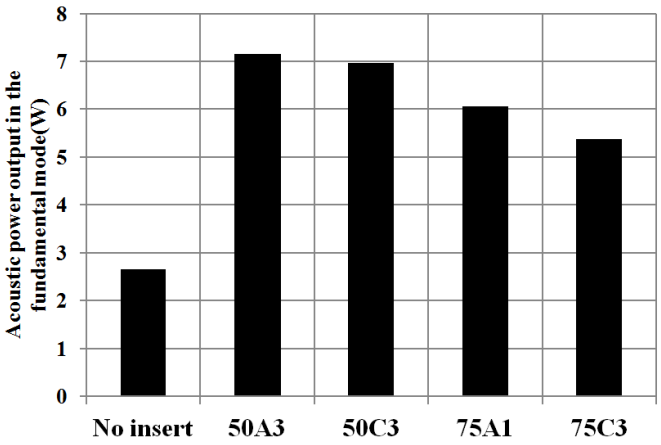

Figure 10: Acoustic power carried out in the fundamental mode in the four inserts considered as compared to the no-insert case. The working fluid is air at atmospheric mean pressure

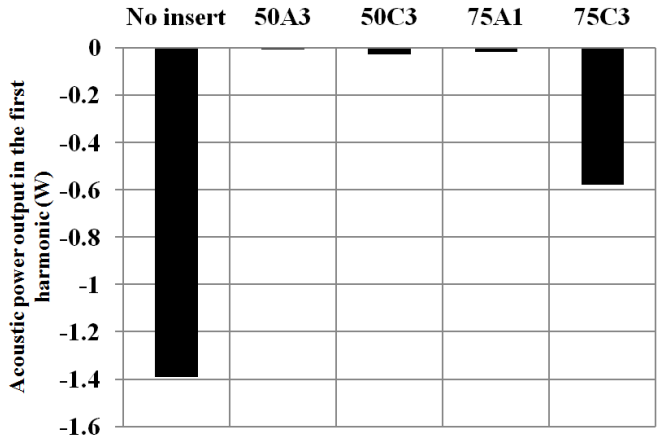

Figure 11: Acoustic power carried out in the first harmonic in the four inserts considered as compared to the no-insert case. The working fluid is air at atmospheric mean pressure

insert is observed to have a better performance with respect to the 75C3 or the 75A1 inserts. The insert 50A3 shows a similar performance to that of the 50C3 insert.

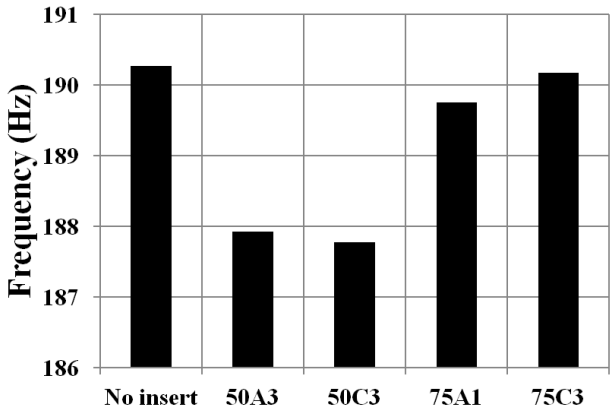

Figure 12: Frequency of operation in the four inserts considered as compared to the no-insert case. The working fluid is air at atmospheric mean pressure

It is of interest to carry some experiments using the 50C3 insert at different axial positions along the resonator and observe the effects on the acoustic power. Figure 13 shows the acoustic power output produced in the fundamental pressure wave, showing that the maximum acoustic power generated occurs when the insert is located at 68 cm from the hot-side blind flange, corresponding to the velocity anti-node of the first harmonics. The acoustic power decreases when the insert is placed nearer or further.

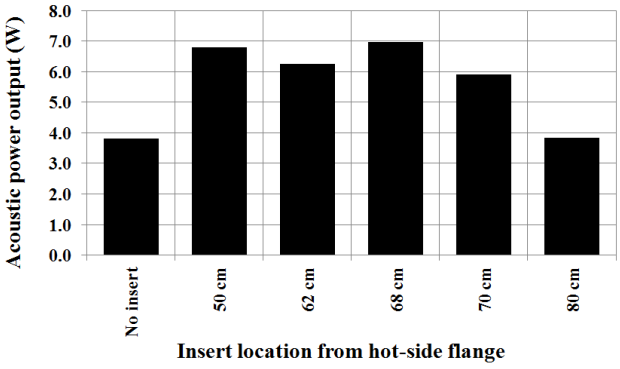

Figure 13: Acoustic power in the fundamental mode using insert 50C3 at different axial positions along the resonator. The working fluid is air at atmospheric mean pressure

4 Summary and conclusion

This work investigates the use of inserts to suppress the generation of harmonics. The work presents evidence that the use of 50C3-68 insert described above positioned at the velocity anti-node of the first harmonic is able to increase the acoustic power carried out in the fundamental mode from 3.4 W to 8.4 W and to reduce the acoustic power carried out in the first harmonic from 1.3 W to 0.1 W. Among three different porosities studied (0.25, 0.5 and 0.75), the porosity of 0.5 is found best. The absolute values of

all dynamic pressure carried out in the fundamental mode as well as in the harmonics are reduced after the placement of the insert. Regression analysis shows linear relationships, with and without insert, for the relationships between P_0^2 and the input heat, P_1 and P_0^2, and P_2 and P_1^2.

References

[1] K. M. Godshalk, C. Jin, Y. K. Kwong, E. L. Hershberg, G. W. Swift, and R. Radebaugh. Characterization of 350 hz thermoacoustic driven orifice pulse tube refrigerator with measurements of the phase of the mass flow and pressure. *Advances in Cryogenic Engineering*, 41:1411–1418, 1996.

[2] D. L. Gardner and G. W. Swift. A cascade thermoacoustic engine. *J. Acoust. Soc. Am.*, 114(4):1905–1919, 2003.

[3] Chao Shen, Yaling He, Yuguang Li, Hanbing Ke, Dongwei Zhang, and Yingwen Liu. Performance of solar powered thermoacoustic engine at different tilted angles. *Applied Thermal Engineering*, 29(13):2745 – 2756, 2009.

[4] Hatazawa Masayasu, Sugita Hiroshi, Ogawa Takashiro, and Seo Yoshitoki. Performance of a thermoacoustic sound wave generator driven with waste heat of automobile gasoline engine. *Transactions of the Japan Society of Mechanical Engineers. B*, 70(689):292 – 299, 2004.

[5] A. H. Ibrahim and E. Abdel-Rahman. Innovative solar-energy-driven power converter: Efficient operation of thermo-acoustic engines. In *The 2nd International Conference on Renewable Energy: Generation and Applications, AlAin, UAE*, 2012.

[6] B.J. Gillman. *A Study of Coupled Thermoacoustic Engines*. PhD thesis, The University of Utah, 2009.

[7] Y. A. Cengel and M. A. Boles. *Thermodynamics: an engineering approach*. McGraw-Hill series in mechanical engineering. McGraw-Hill Higher Education, 2006.

[8] M. A. Nouh, N. M. Arafa, K. Larsson, and E. Abdel-Rahman. Design study of anharmonic standing wave thermoacoustic heat engine. In *The Sixteenth International Conf. on Sound and Vibration. KraKow, Poland*, 2009.

[9] E.C. Luo, H. Ling, W. Dai, and G.Y. Yu. Experimental study of the influence of different resonators on thermoacoustic conversion performance of a thermoacoustic-stirling heat engine. *Ultrasonics*, 44:e1507 – e1509, 2006.

[10] D. L. Gardner and G.W. Swift. Experimental verification of a two-sensor acoustic intensity measurement in lossy ducts. *Journal of the Acoustical Society of America*, 124(3):1584 – 1590, 2008.

[11] G. W. Swift. Thermoacoustic engines. *Journal of the Acoustical Society of America*, 84(4):1145–1180, 1988.

[12] G. W. Swift. Analysis and performance of a large thermoacoustic engine. *Journal of the Acoustical Society of America*, 92(3):1551–1563, 1992.

[13] A.H. Ibrahim, M. Emam, Hosny Omar, K. Addas, and E. Abdel-Rahman. Performance evaluation of thermoacoustic engine using different gases. In *Proceedings of ICSV19, Vilnius, Lithuania*, 2012.

[14] A. H. Ibrahim, A. A. Elbeltagy, M. Emam, and E. Abdel-Rahman. Development and analysis of non-linearity in the pressure waves resulting from thermoacoustic heat engines. In *Acoustics 2012, Nantes, France*, 2012.